JOURNAL OF AIRCRAFT
Vol. 45, No. 2, March–April 2008

Design Tailoring for Pressure Pillowing Using Tow-Placed Steered Fibers

Ahmad Alhajahmad,* Mostafa M. Abdalla,† and Zafer Gürdal‡
Delft University of Technology, 2629 HS Delft, The Netherlands

DOI: 10.2514/1.32676

Manufacturing of high-quality fiber-reinforced composite structures with spatially varying fiber orientation is possible using advanced tow-placement machines. Changing the fiber-orientation angle within a layer produces variable-stiffness properties. Contrary to traditional composites with straight fibers, this method allows the designer to fully benefit from the directional material properties of the composite to improve laminate performance by determining optimal fiber paths. In this paper, design tailoring for the pressure-pillowing problem of a fuselage skin is addressed using steered fibers. The problem is modeled as a two-dimensional plate using von Kármán plate equations. The analysis is performed using the Rayleigh–Ritz method, and the nonlinear response is traced using a normal flow algorithm. The design objective is to determine the optimal fiber paths over the panel for maximum failure load. Different designs are obtained for different loading cases. The results indicate that by using steered fibers, the pressure-pillowing problem can be alleviated and the load-carrying capacity of the structure can be improved, compared with designs using straight fibers.

Nomenclature

A_{ij}	=	in-plane stiffnesses
a, b	=	length and width of the plate
D_{ij}	=	bending stiffnesses
F	=	failure index
m, n	=	number of basis functions in the x and y directions, respectively
N	=	total number of plies
n_t	=	number of terms
t	=	ply thickness
u^0, v^0, w	=	displacement along the x, y, and z directiosn
ε_x, ε_y, γ_{xy}	=	engineering strains along the global axis
$\boldsymbol{\kappa_x}$, $\boldsymbol{\kappa_y}$, $\boldsymbol{\kappa_{xy}}$	=	curvatures
λ	=	scaling load factor
λ^f	=	failure load
σ_1, σ_2, σ_{12}	=	stresses in the principal material directions
Φ_i^u, Φ_i^v, Φ_i^w	=	assumed functions for u^0, v^0, and w
Π	=	total potential of the plate

I. Introduction

ONE of the primary advantages of using fiber-reinforced laminated composites in structural design is the ability to change the stiffness and strength of the laminate by designing the laminate stacking sequence to improve its performance. This flexibility to design the stacking sequence of the laminate is typically referred to as laminate tailoring. Tailoring is traditionally achieved by keeping the fiber-orientation angle within each layer constant throughout a component, resulting in a constant-stiffness structure. By limiting each layer to a single orientation over the entire component, the designer is unable to fully exploit the directional material properties offered by advanced composites. A simple method for improved tailoring is the introduction of discrete jumps in the laminate construction by adding patches of additional layers with different fiber orientations into the component. For example, Biggers et al. [1,2] achieved tailoring by redistributing the layers with specified orientations across the planform of rectangular plates to create beneficial stiffening patterns against compression and shear buckling. Another method of creating a variable-stiffness composite structure is by changing the fiber-orientation angle continuously within the lamina. Allowing the fibers to curve within the lamina constitutes an advanced tailoring option to account for nonuniform stress states in a continuous manner. By varying the stiffness properties of composite laminates from one point to another, the design space is expanded, compared with the classical stacking-sequence design problem. As a consequence, stiffer and/or lighter structures can be obtained.

An intensive study of rectangular panels with curvilinear fiber paths, termed variable-stiffness panels, was carried out by Gürdal and Olmedo [3]. The curvilinear paths in those studies were generated from a base curve that changes its orientation angle linearly from one end of the panel to the other, while taking into account constraints on the radius of curvature of the fiber paths. Despite the fact that linear fiber-orientation variation represents only a limited class of spatially varying orientations, earlier studies showed that significant improvements in the laminate response can be obtained for panels with and without holes under compression and shear loads [4–6]. Investigation of the optimal designs for both constant- and variable-stiffness rectangular composite plates for minimum compliance was performed by Setoodeh et al. [7]. In those studies, the lamination parameters were used as design variables instead of fiber-orientation angles, thus reducing the number of design variables. Moreover, the formulation guaranteed an optimal solution, benefiting from the fact that the optimization problem is convex. Although the actual stacking sequence was unknown, the results showed that substantial improvements in stiffness can be gained by using variable-stiffness designs. In a follow-up work, the curvilinear fiber paths were generated from the lamination parameter distribution [8].

A challenging problem in aircraft structures associated with thin-walled stiffened structures is the so-called pressure pillowing. Pressurized fuselages and fuel tanks are typical examples of structures in which pressure pillowing is observed. In the case of fuselages, the cabin pressure causes a significant pressure differential across the skin. An unstiffened fuselage would carry this internal pressure load as a shell in membrane response, as with pressure vessels. However, internal longitudinal and transverse stiffeners

Received 7 June 2007; revision received 2 September 2007; accepted for publication 15 October 2007.

*Ph.D. Student, Aerospace Structures Group, Faculty of Aerospace Engineering, Kluyverweg 1.
†Assistant Professor, Aerospace Structures Group, Kluyverweg 1. Member AIAA.
‡Professor, Aerospace Structures Chair, Kluyverweg 1. Associate Fellow AIAA.

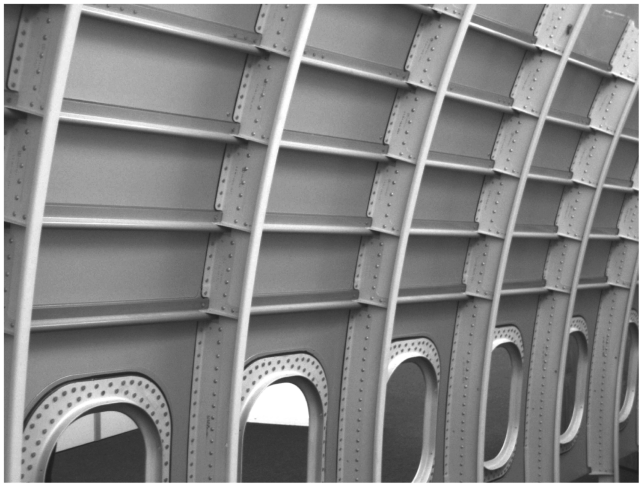

Fig. 1 Stiffened structure of a pressurized fuselage (courtesy of the Fiber Metal Laminates Center of Competence at Delft University of Technology).

(stringers and frames, as shown in Fig. 1) are necessary to carry maneuver loads. The presence of these stiffeners prevents the fuselage skin from expanding as a membrane, and the skin bulges, or "pillows," within each panel bay under the action of the internal pressure. When the skin is restrained against out-of-plane expansion at the stiffener locations, a bending boundary layer is formed.

An experimental and analytical study of the nonlinear response and failure characteristics of internally pressurized constant-stiffness composite fuselage panels with clamped edges was performed by Boitnott et al. [9]. The study showed that the graphite-epoxy specimens failed at their edges (where the magnitudes of local bending gradients and interlaminar stresses are maximum). Recently, design tailoring for pressure pillowing using the variable-stiffness concept was investigated by Alhajahmad et al. [10]. The pressure-pillowing problem was modeled as a one-dimensional clamped–clamped beam plate in two loading cases. The first case was a one-dimensional plate subjected to pressure, and the second case was a one-dimensional plate under combined pressure and in-plane compressive loads. For both loading cases, the optimal fiber paths along the beam-plate length for minimum weight subject to strength constraints were determined. It was shown in the latter study that by using steered fibers, the pressure-pillowing problem can be alleviated and lighter laminates can be designed than with designs using straight fibers.

For the analysis of the pressure-pillowing problem, the fuselage skin of a panel bay can be modeled using different levels of complexity. Research reported in [10] used a simple beam-plate model but, in general, required a two-dimensional plate or shallow shell modeling under combined pressure and in-plane loads. Hence, in this paper, the problem is modeled as a two-dimensional plate subjected to pressure and in-plane loads. The optimization problem is formulated to determine the optimal fiber paths over the panel for maximum failure load. For optimization purposes, it is of great importance to select an efficient and fast method for the nonlinear analysis. Although the finite element method (FEM) is a powerful tool for structural analysis problems, the nonlinear nature of the problem at hand makes the use of the FEM undesirable, due to excessive computational time required. In this study, the plate problem is approximated using the Rayleigh–Ritz method (R–R), and the nonlinear response is traced using a normal flow algorithm [11].

II. Problem Formulation

In this paper, a pressurized fuselage skin bounded by two stringers and two frames is modeled as a two-dimensional plate. It is assumed that the skin is flat, balanced, and symmetric laminate with a variable-stiffness layup $[\pm\theta(x, y)]_{ns}$. The laminate is loaded in two steps. In the first loading step, a uniform pressure p is applied, which is approximately translated into two loads, axial tensile load F_x and hoop tensile load F_y, calculated as

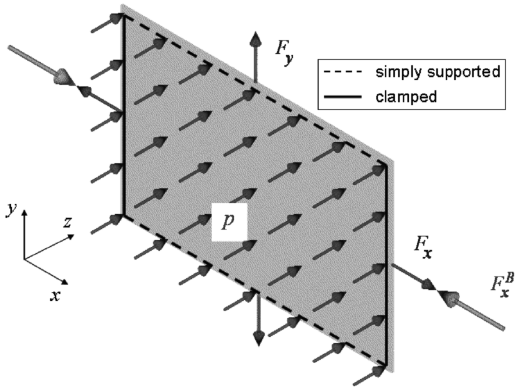

Fig. 2 Fuselage panel model.

$$F_x = \frac{pR}{2}b \qquad F_y = pRa \tag{1}$$

where a and b are the length and the width of the plate, respectively, and R is the radius of the fuselage. The pressure and, hence, the tensile loads are incremented by means of a scaling factor λ_1 in the first loading step. It should be noted that the relations given by Eqs. (1) are valid only for unstiffened cylindrical shells, because the skin loads will be reduced according to the stiffness contributions from the stringers and frames. However, for the sake of simplicity, these contributions are neglected in the present study. For a given fuselage with known ring and longitudinal stiffeners, their affect on the skin loads can easily be incorporated. In principle, the averaged applied loads will also change, because some of the skin panels might buckle, resulting in load redistribution. Such interactions, however, require a consideration of the complete structure, not of a single panel, and are beyond the scope of the present work. In the second loading step, an additional axial compressive load F_x^B, which results from fuselage bending, is applied. This latter load is incremented by means of a scaling factor λ_2, while keeping λ_1 fixed at the end of the first loading step.

The panel boundary conditions are clamped at $x = 0$ and $x = a$, simulating the panel edges at the frame locations, and are simply supported at $y = 0$ and $y = b$, simulating the panel edges at the stringer locations. The fuselage panel model is shown in Fig. 2.

III. Analysis Formulation

Assuming that the plate is thin, such that the Kirchhoff hypothesis is valid, the laminate strains are expressed in the following form [12]:

$$\{\boldsymbol{\varepsilon}\} = \{\boldsymbol{\varepsilon}^0\} + z\{\boldsymbol{\kappa}\} \tag{2}$$

where $\{\boldsymbol{\varepsilon}^0\}$ and $\{\boldsymbol{\kappa}\}$ denote the midplane strains and curvatures, respectively. In the moderately large rotation case, according to the von Kármán model, the midplane strains and curvatures are given by

$$\{\boldsymbol{\varepsilon}^0\} = \begin{Bmatrix} \varepsilon_x^0 \\ \varepsilon_y^0 \\ \gamma_{xy}^0 \end{Bmatrix} = \begin{Bmatrix} \frac{\partial u^0}{\partial x} + \frac{1}{2}\left(\frac{\partial w}{\partial x}\right)^2 \\ \frac{\partial v^0}{\partial y} + \frac{1}{2}\left(\frac{\partial w}{\partial y}\right)^2 \\ \frac{\partial u^0}{\partial y} + \frac{\partial v^0}{\partial x} + \frac{\partial w}{\partial x}\frac{\partial w}{\partial y} \end{Bmatrix} \tag{3}$$

$$\{\boldsymbol{\kappa}\} = \begin{Bmatrix} \kappa_x \\ \kappa_y \\ \kappa_{xy} \end{Bmatrix} = \begin{Bmatrix} -\frac{\partial^2 w}{\partial x^2} \\ -\frac{\partial^2 w}{\partial y^2} \\ -2\frac{\partial^2 w}{\partial x \partial y} \end{Bmatrix} \tag{4}$$

where u^0, v^0, and w are the midplane displacements.

Following the Rayleigh–Ritz procedure [13], the total potential energy is given by

$$\Pi = U - W \tag{5}$$

where U is the strain energy, and W is the potential energy of the external loads. For symmetric and balanced laminates, the strain energy in terms of the midplane strains and curvatures is given by

$$\begin{aligned} U = \frac{1}{2}\int_0^a \int_0^b [&A_{11}(\varepsilon_x^0)^2 + A_{22}(\varepsilon_y^0)^2 + 2A_{12}\varepsilon_x^0\varepsilon_y^0 + A_{66}(\gamma_{xy}^0)^2 \\ &+ D_{11}\kappa_x^2 + D_{22}\kappa_y^2 + 2D_{12}\kappa_x\kappa_y + 2D_{16}\kappa_x\kappa_{xy} + 2D_{26}\kappa_y\kappa_{xy} \\ &+ D_{66}\kappa_{xy}^2]\,\mathrm{d}x\,\mathrm{d}y \end{aligned} \tag{6}$$

where A_{ij} and D_{ij} are the in-plane and out-of-plane stiffnesses, respectively. For straight-fiber panels, the A_{ij} and D_{ij} may be moved out of the integral because they are independent of x and y. However, for variable-stiffness panels, the A_{ij} and D_{ij} are functions of the panel coordinates and must remain as part of the integrand.

The potential energy of the external loads is given by

$$W = \lambda_1\left[F_x u^0_{(x=a)} + F_y v^0_{(y=b)} + p\int_0^a\int_0^b w\,\mathrm{d}x\,\mathrm{d}y\right] + \lambda_2 F_x^B u^0_{(x=a)} \tag{7}$$

The displacement functions are assumed as follows:

$$\begin{aligned} &w(x,y) = \sum_{i=1}^{n_t} a_i\Phi_i^w \qquad u^0(x,y) = b_0\frac{x}{a} + \sum_{i=1}^{2n_t} b_i\Phi_i^u \\ &v^0(x,y) = c_0\frac{y}{b} + \sum_{i=1}^{2n_t} c_i\Phi_i^v \end{aligned} \tag{8}$$

where n_t is the number of terms; a_i, b_i, and c_i are the Ritz coefficients; and $b_0 = u^0_{(x=a)}$ and $c_0 = v^0_{(y=b)}$ represent the edge displacements.

Depending on the choice of the functions Φ_i^w, Φ_i^u, and Φ_i^v, different boundary conditions can be modeled. Because the panel edges are bounded by different structural elements such as stringers, frames, and other adjacent panels, the boundary conditions can be very complex. In the current work, we assume linearly varying deformable straight edges clamped at $x = 0$ and $x = a$ and simply supported at $y = 0$ and $y = b$. This implies that the out-of-plane displacement of the stringers due to bending will be neglected. The boundary conditions can be summarized as follows:

At $x = 0$,

$$u^0(0,y) = 0 \qquad v^0(0,y) = c_0\frac{y}{b} \qquad w(0,y) = 0 \qquad w_{,x}(0,y) = 0$$

At $x = a$,

$$u^0(a,y) = b_0 \qquad v^0(a,y) = c_0\frac{y}{b} \qquad w(a,y) = 0 \qquad w_{,x}(a,y) = 0$$

At $y = 0$,

$$v^0(x,0) = 0 \qquad u^0(x,0) = b_0\frac{x}{a} \qquad w(x,0) = 0$$

At $y = b$,

$$v^0(x,b) = c_0 \qquad u^0(x,b) = b_0\frac{x}{a} \qquad w(x,b) = 0$$

where a subscript comma indicates a derivative with respect to the variable following it.

For the assumed boundary conditions, the displacement field is given by

$$\begin{aligned} &w(x,y) = \sum_{i=1}^{n_t}\sum_{j=1}^{n_t} a_{ij}\left(\cos\frac{(i-1)\pi x}{a} - \cos\frac{(i+1)\pi x}{a}\right)\sin\frac{j\pi y}{b} \\ &u^0(x,y) = b_0\frac{x}{a} + \sum_{i=1}^{2n_t}\sum_{j=1}^{2n_t} b_{ij}\sin\frac{i\pi x}{a}\sin\frac{j\pi y}{b} \\ &v^0(x,y) = c_0\frac{y}{b} + \sum_{i=1}^{2n_t}\sum_{j=1}^{2n_t} c_{ij}\sin\frac{i\pi x}{a}\sin\frac{j\pi y}{b} \end{aligned} \tag{9}$$

Note that the number of the assumed terms for in-plane displacements u^0 and v^0 is twice that of out-of-plane displacement in w. This is done to ensure that the in-plane equilibrium is adequately satisfied.

By using the stationary conditions of total potential and minimizing with respect to Ritz coefficients a_i, b_i, and c_i,[§] we obtain the general equilibrium equations for a symmetric and balanced laminated composite plate (see the Appendix for details):

$$\begin{aligned} &-(\lambda_1 F_x + \lambda_2 F_x^B) + K_{il}^{ub} b_i + K_{il}^{uc} c_i + K_{ijl}^{uaa} a_i a_j = 0 \\ &-\lambda_1 F_y + K_{il}^{vb} b_i + K_{il}^{vc} c_i + K_{ijl}^{vaa} a_i a_j = 0 \\ &K_{il} a_i + K_{ikl}^{wba} b_i a_k + K_{ikl}^{wca} c_i a_k + K_{ijkl}^{waaa} a_i a_j a_k - \lambda_1 \mathrm{P}_l = 0 \end{aligned} \tag{10}$$

The first two equations in Eqs. (10) are linear in the Ritz coefficients b_i and c_i. Thus, the preceding three equations can be reduced to a single nonlinear equation by eliminating b_i and c_i from the third equation, using the first two equations. Then the final set of nonlinear equations that define an equilibrium load-deflection path is solved for a_i, and by back substitution, the coefficients b_i and c_i are computed. Different techniques are available for the tracing of nonlinear equilibrium paths [14]. In this paper, we use the normal flow algorithm because of its robustness and efficiency [14].

IV. Failure Analysis

The failure load λ^f is defined as the load level at which first failure occurs. For the purpose of predicting failure, we use the Tsai–Wu failure criterion. For an orthotropic lamina under plane stress conditions, this criterion is given by

$$F = F_{11}\sigma_1^2 + 2F_{12}\sigma_1\sigma_2 + F_{22}\sigma_2^2 + F_{66}\sigma_{12}^2 + F_1\sigma_1 + F_2\sigma_2 \tag{11}$$

where F is the failure index; σ_1, σ_2, and σ_{12} are the in-plane stresses in the principal material directions; and F_{ij} are functions expressed in terms of the strength properties, as follows:

$$\begin{aligned} &F_{11} = \frac{1}{X_t X_c} \qquad F_{22} = \frac{1}{Y_t Y_c} \qquad F_{66} = \frac{1}{S^2} \qquad F_1 = \frac{1}{X_t} - \frac{1}{X_c} \\ &F_2 = \frac{1}{Y_t} - \frac{1}{Y_c} \qquad F_{12} = \frac{1}{2X_t^2}[1 - X_t(F_1 + F_2) - X_t^2(F_{11} + F_{22})] \end{aligned} \tag{12}$$

According to the Tsai–Wu criterion, a composite fails when the following condition is violated:

$$F \le 1 \tag{13}$$

To apply the Tsai–Wu criterion to variable-stiffness laminates, it must be recognized that stresses will vary as a function of location over the domain. This requires that the condition in Eq. (13) must be satisfied at every point of every ply throughout the structure; that is,

$$F_{(x,y)} \le 1 \tag{14}$$

[§]Note that the matrix a_{ij} was converted to a vector a_i containing the elements of a_{ij} row by row; for example, for $n_t = 2$, $a_1 = a_{11}$, $a_2 = a_{12}$, $a_3 = a_{21}$, and $a_4 = a_{22}$. The same conversion applies to b_{ij} and c_{ij}

V. Optimization Formulation

The objective of the optimization problem can be formulated either to minimize the weight of the structure for given applied loads or to maximize the failure load for a given thickness. In this paper, the goal of the optimization problem is to determine the optimal distribution of the fiber-orientation angles (or the fiber paths) over the structure for maximum failure load. Mathematically, the problem is formulated as

$$\text{maximize } \lambda^f(X) \tag{15}$$

where λ^f is the objective function representing different loading cases, and X is a vector of design variables.

Varying the stiffness throughout the structure requires defining the fiber-orientation variations. Hence, for the vector of design variables, a discretization of the fiber-orientation angle was adopted. In earlier investigations, a two-parameter linear orientation variation was considered. More recently, multiparameter functions with more general nonlinear fiber-orientation variation have been used [10]. In the next sections, linear and nonlinear variations of fiber-orientation angles will be described.

A. Linear Variation of Fiber-Orientation Angles

Simple forms of linear variation of fiber-orientation angles for rectangular panels have been described in the literature [3]; for example,

$$\theta(\tilde{x}) = \frac{2(T_1 - T_0)}{a}|\tilde{x}| + T_0 \tag{16}$$

where T_0 is the fiber-orientation angle at the panel center ($\tilde{x} = 0$), and T_1 is the fiber-orientation angle at the panel ends ($\tilde{x} = \pm a/2$). To make use of Eq. (16), considering the coordinate system defined in Fig. 2, we write Eq. (16) as

$$\theta(x) = \begin{cases} \frac{2}{a}(T_0 - T_1)x + T_1 & \text{for } 0 \le x \le \frac{a}{2} \\ \frac{2}{a}(T_1 - T_0)x + T_1 - 2(T_1 - T_0) & \text{for } \frac{a}{2} \le x \le a \end{cases} \tag{17}$$

B. Nonlinear Variation of Fiber-Orientation Angles

In a previous study [10], a definition of a unidirectional variation based on a nonlinear function for the fiber-orientation angle was introduced. The nonlinear function was defined using Lobatto–Legendre polynomials. The definition of unidirectional variation can be generalized to be applied to spatially varying fiber-orientation angles, as demonstrated in this section.

Assume a rectangular domain, as shown in Fig. 3. We define the normalized coordinates ξ and η as follows:

$$\xi = \frac{2x - a}{a} \qquad \eta = \frac{2y - b}{b} \tag{18}$$

such that $-1 \le \xi \le 1, -1 \le \eta \le 1$.

We define the fiber-orientation angle in the ξ–η plane by

$$\theta(\xi, \eta) = \sum_{i=0}^{m-1} \sum_{j=0}^{n-1} T_{ij} L_i(\xi) L_j(\eta) \tag{19}$$

where m and n are the number of basis functions used in the ξ and η directions, respectively; T_{ij} are unknown coefficients; and L_i are the Lobatto polynomials, defined as

$$L_i(\xi) = \int_{-1}^{\xi} P_{i-1}(\mu)\, \mathrm{d}\mu \qquad i \ge 2 \tag{20}$$

where $L_0(\xi) = 1$ and $L_1(\xi) = \xi$ or, in a recursive form,

$$L_i(\xi) = \frac{1}{i}(\xi P_{i-1}(\xi) - P_{i-2}(\xi)) \qquad i \ge 2 \tag{21}$$

where P_i are the Legendre polynomials given by

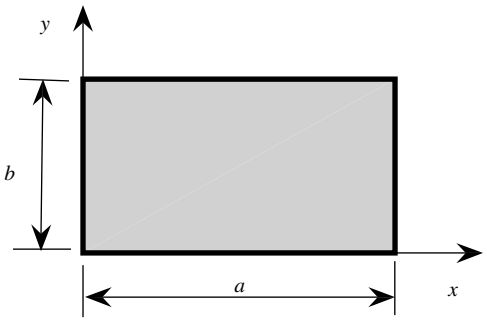

Fig. 3 Rectangular domain and coordinate system.

$$P_i(\xi) = [(2i - 1)\xi P_{(i-1)} - (i - 1)P_{(i-2)}]/i \qquad i \ge 2 \tag{22}$$

and where $P_0(\xi) = 1$ and $P_1(\xi) = \xi$.

For example, the first few Lobatto polynomials are

$$L_2(\xi) = \tfrac{1}{2}(\xi^2 - 1) \qquad L_3(\xi) = \tfrac{\xi}{2}(\xi^2 - 1)$$
$$L_4(\xi) = \tfrac{1}{8}(1 - 6\xi^2 + 5\xi^4) \qquad L_5(\xi) = \tfrac{1}{8}\xi(3 - 10\xi^2 + 7\xi^4)$$

By increasing the number of coefficients T_{ij} in Eq. (19), more freedom can be achieved to represent the fiber-orientation-angle variations. Consequently, there is better chance to capture the optimal fiber-angle distribution. Therefore, in this study, the design variables are the unknown coefficients T_{ij}. To insure a local balanced laminate condition, in the present paper, a stack of two layups with either $[\pm\theta(x)]_{ns}$ or $[\pm\theta(x, y)]_{ns}$ laminates is considered, even though only the fiber-angle distribution for a single layer is designed.

VI. Application and Results

Numerical results are generated for a symmetric and balanced laminate with the variable-stiffness layup $[\pm\theta(x, y)]_{4s}$. The number of laminate plies is $N = 16$. Each ply has a constant thickness of $t = 0.01$ in. (i.e., the total thickness is $h = Nt$). The composite material is typical graphite-epoxy, with stiffness and strength properties given in Table 1 [15]. The pressure load is $p = 15$ psi and the fuselage radius is $R = 100$ in. The underlying goal of the optimization problems is to determine the optimal fiber paths over the structure for maximum failure load.

The results presented in this paper are for a number of assumed terms $n_t = 3$, which gives adequate accuracy when compared with finite element analysis. The nonlinear analysis is verified with that of commercial finite element package Abaqus using the S4R element. The initial loads F_x and F_y are proportional to the pressure load, as stated earlier, and the subsequently applied compressive load is $F_x^B = -2F_x$. The values of the stresses in the principal material directions are compared for different designs. For the upper ply ($z = h/2$, on the outside surface of the fuselage) and for the lower ply ($z = -h/2$, on the inside surface of the fuselage) of a square panel ($a/b = 1$), the stresses at the panel center as functions of the load factor are shown in Figs. 4 and 5, respectively. It is clear that the developed Rayleigh–Ritz analysis model agrees well with the finite element analysis. It was found that the maximum error, in terms of

Table 1 Material properties

Material properties	Values
E_1	30×10^6 psi
E_2	0.75×10^6 psi
ν_{12}	0.25
G_{12}	0.375×10^6 psi
X_t	150×10^3 psi
Y_t	6×10^3 psi
S	10×10^3 psi
X_c	100×10^3 psi
Y_c	17×10^3 psi

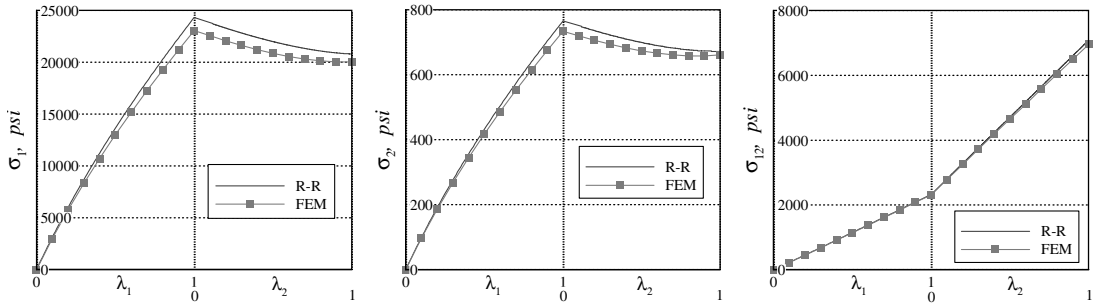

Fig. 4 Stresses in the principal material directions of the $[\pm 45\,\mathrm{deg}]_{4s}$ design using the R–R and FEM; $z = h/2$.

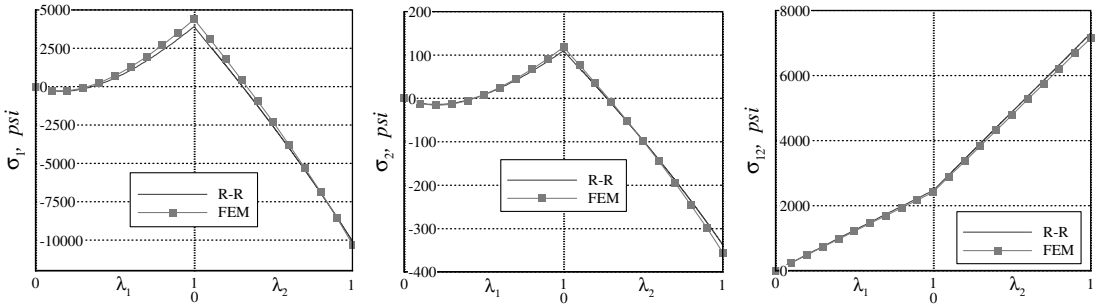

Fig. 5 Stresses in the principal material directions of the $[\pm 45\,\mathrm{deg}]_{4s}$ design using the R–R and FEM; $z = -h/2$.

stresses, is within less than 10%, which makes it adequate for preliminary design purposes.

In this paper, two loading cases are considered. The first loading case is a square plate ($a/b = 1$) subjected to pressure only (no pressure-induced tensile loads) which will be called case I, and the second case is a plate subjected to a combination of pressure and in-plane tensile and compressive loads applied in two steps, as described earlier. In the first loading step, the pressure and the pressure-induced tensile loads are applied. Then the in-plane compressive load is applied in the second loading step, while keeping the loads applied in the first loading step constant. This latter case will be called case II, in which two aspect ratios will be addressed: $a/b = 1$ and $a/b = 2$.

A. Case I: Square Plate Subjected to Pressure

To better understand the developed designs, the fiber-orientation angle will initially be varied as a function of x only, $\theta = \theta(x)$, and then it will be varied spatially as a function of both the x and y coordinates, $\theta = \theta(x, y)$.

1. Linear Variation of Fiber-Orientation Angles, $\theta = \theta(x)$

In this particular case, the design space has only two variables. Therefore, instead of doing optimization, the design space is first studied graphically. We first analyze the plate using linear variation of the fiber-orientation angles given by Eq. (17). The pressure failure load is calculated parametrically for various combinations of the angles T_0 and T_1 in the range of $0\,\mathrm{deg} \le \theta \le 90\,\mathrm{deg}$. The results of this study are shown in Fig. 6, in which the failure load is plotted as a function of T_0 and T_1.

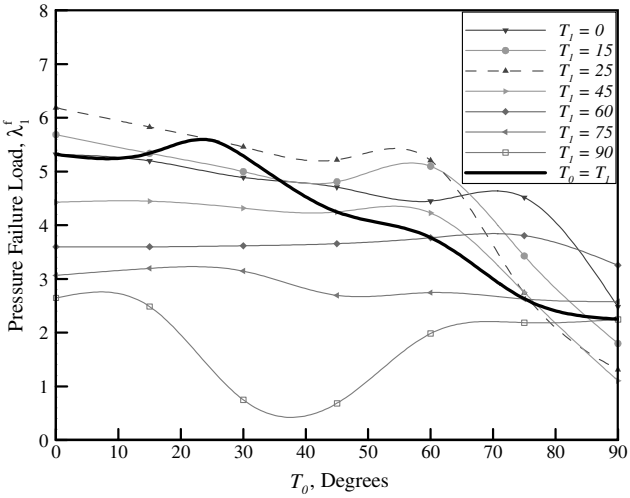

Fig. 6 Case-I pressure failure load performance using linear variation of fiber-orientation angles.

The thick line in the figure is for constant-stiffness straight-fiber format panels. For variable-stiffness panels, a family of curves corresponding to various values of T_0 and T_1 is shown in Fig. 6. Each curve is generated by varying the value of T_0 between 0 and 90 deg for a given value of T_1, as labeled in the figure. Intersection of these curves with the curve for the straight-fiber panel is a panel for which T_0 is equal to the T_1 value. Clearly, for constant-stiffness laminates,

Table 2 Case-I load-carrying-capacity improvement (steered fiber vs straight fiber); $\theta = \theta(x)$.

Design type	No. of design variables	Failure load λ_1^f	Load-carrying capacity improvement, %
Constant stiffness $[\pm 25\,\mathrm{deg}]_{4s}$	——	5.56	——
Variable stiffness (linear variation)	2	6.19	10.2
Variable stiffness	5	6.51	14.6
Variable stiffness	8	6.87	19.0

Table 3 Case-I load-carrying-capacity improvement (steered fiber vs straight fiber); $\theta = \theta(x, y)$.

Design type	No. of design variables, $m \times n$	Failure load λ_2^f	Load-carrying capacity improvement, %
Constant stiffness $[\pm 25\ \text{deg}]_{4s}$	——	5.56	——
Variable stiffness	4×4	6.65	16.4
Variable stiffness	5×5	6.95	20.0
Variable stiffness	6×6	7.43	25.2

the maximum failure load is achieved for a $[\pm 25\ \text{deg}]_{4s}$ laminate and the corresponding failure load is $\lambda_1^f = 5.56$. However, the maximum failure load that can be achieved for a variable-stiffness configuration is $\lambda_1^f = 6.19$, and it is obtained for $T_0 = 0$ deg and $T_1 = 25$ deg. This value is about 10% higher than the maximum value obtained with a straight-fiber configuration.

It can also be observed from Fig. 6 that for a given value of T_0, the values of the failure load do not increase monotonically when the values of T_1 increase. Therefore, search for an optimal solution using traditional gradient-based approaches are likely to be trapped in local optima. Accordingly, the simplex method[¶] is used as the design optimization platform. Because this method uses only function value information in the search for optima, the search is repeated with different initial points to avoid getting stuck in local optima.

2. *Nonlinear Variation of Fiber-Orientation Angles, $\theta = \theta(x)$*

The optimization problem is solved using different numbers of design variables (coefficients T_{ij}) using the fiber-orientation variation given by Eq. (19) after setting the terms that include y to zero. The improvement in the load-carrying capacity obtained using the steered-fiber designs compared with the straight-fiber design is shown in Table 2.

The number of design variables is increased until the load-carrying-capacity improvement becomes insignificant. The optimal fiber-orientation distributions for different numbers of design variables, as well as the best design obtained using the linear variation, are shown in Fig. 7.

3. *Nonlinear Variation of Fiber-Orientation Angles, $\theta = \theta(x, y)$*

Varying the fiber orientation spatially as a function of x and y gives more freedom to the fibers to curve within the lamina and, consequently, additional improvement in the load-carrying capacity may be achieved. A comparison between the constant-stiffness and the variable-stiffness designs is shown in Table 3 for different numbers of design variables. The optimal distribution of the fiber-orientation angles for $m = n = 6$ (36 coefficients) is depicted in Fig. 8. To generate the fiber paths from the fiber-orientation distribution, the streamline analogy (or fluid flow analogy) was used [16]. The streamline analogy assumes that each streamline represents the centerline of a course (band of tows or fibers) or, if the course width is made infinitely small, each streamline will represent a single fiber. The optimal fiber paths obtained by using the streamline analogy for $m = n = 6$ are depicted in Fig. 9.

It is clear that the fiber-orientation distribution that results from the use of 6×6 coefficients in the fiber-angle expansion produces the maximum pressure failure load, providing a load-carrying-capacity improvement of 25% over the optimal straight-fiber design. It can also be observed that the fiber-orientation variation (or, in other words, the stiffness variation) is higher within the bending boundary layer (in the vicinity of the clamped edges, where the bending moment is large) than the stiffness variation in the center section of the panel, in which the stiffness is almost constant.

To demonstrate the values of the fiber-orientation angles that are now functions of both x and y, the fiber orientations are plotted as functions of x at two different sections in the panel: $y/b = 0$ and $y/b = 0.5$. The fiber-orientation distributions at those sections, along with that for the x direction variation with eight coefficients, are shown in Fig. 10. It is clear that the fiber-orientation distribution at $y/b = 0$ is asymmetric about $x/a = 0.5$, whereas it becomes symmetric at $y/b = 0.5$, showing a similar trend to the fiber-orientation distribution for $\theta = \theta(x)$, with slight variations of the fiber-orientation angles away from the clamped edges.

To demonstrate the mechanism that helps improve the load-carrying capacity of the variable stiffness laminate, the distributions of stresses and the failure indices for both straight-fiber and steered-fiber designs over the entire panel in the upper layer of the laminate ($z = h/2$, where the failure first occurs) are plotted in Figs. 11 and 12 at their corresponding failure load levels.

It can be seen from the stress plots that the values of the stresses σ_1 for both designs (straight fiber and steered fiber) are much higher than those for σ_2 and σ_{12}. It can also be observed that the level of the compressive stresses σ_1 near the clamped edges is comparable for

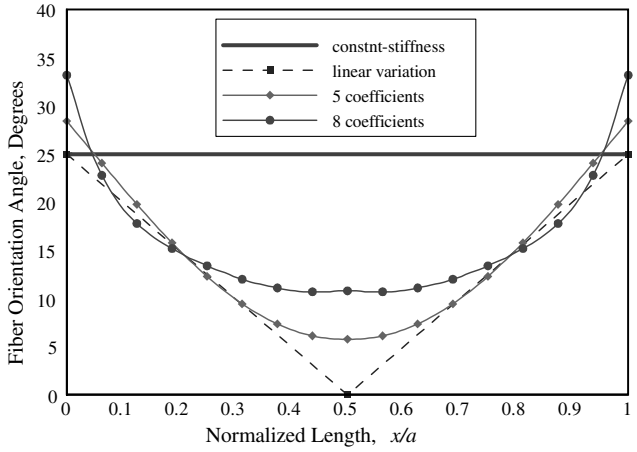

Fig. 7 Case-I optimal distributions of the fiber-orientation angles; $\theta = \theta(x)$.

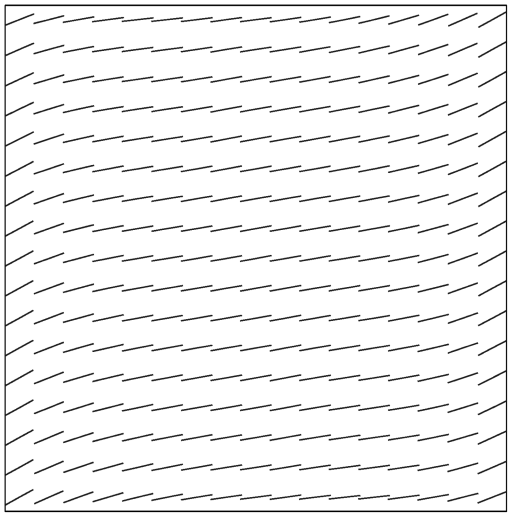

Fig. 8 Case-I optimal distribution of the fiber-orientation angles for maximum failure load.

[¶]From the Microsoft International Mathematics and Statistics Library, using Fortran 90 subroutine DUMPOL, minimize a function of N variables using a direct search polytope algorithm.

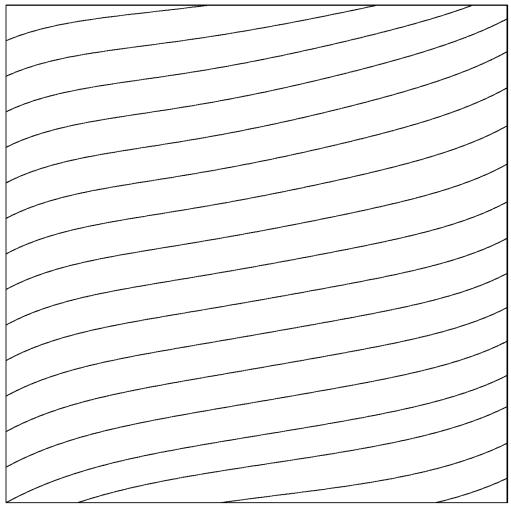

Fig. 9 Case-I optimal fiber paths for maximum failure load.

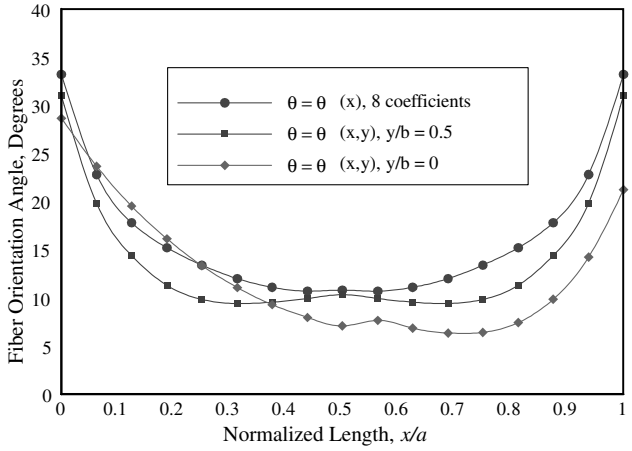

Fig. 10 Case-I fiber-orientation distributions for $\theta = \theta(x)$ and $\theta = \theta(x, y)$ at different sections.

both designs, despite the fact that the load level difference is 25%. On the other hand, the level of the tensile stresses σ_1 for the steered-fiber design is higher than that for the straight-fiber design in the center section of the panel. For the stresses σ_2 and σ_{12}, similar distributions with different values are shown for both designs. The 25% increase in the load-carrying capacity over the constant-stiffness design, obtained for the variable-stiffness design, is mainly due to the stress redistribution throughout the panel, achieved by the steered fibers. This is visually observable from the plots of the Tsai–Wu failure index, in which for the constant-stiffness laminate design, the most critical stress state is localized near the clamped-edge locations, whereas for the steered fibers, the critical locations are more uniformly distributed over the panel, as shown in Fig. 12d. The more uniform distribution of the failure index at this 25%-higher load level may be perceived to make the panel more prone to failure. However, the same change can be interpreted that if the panel is loaded at the level of the straight-fiber design, then the concentration of the failure index at the panel edges is eliminated.

B. Case II: Plate Subjected to Pressure, Tensile, and Compressive Loads

In this case, it is assumed that the pressure and the pressure-induced tensile loads are kept constant ($\lambda_1 = 1$) after the first loading step, and the compressive load $F_x^B = -2\lambda_2 F_x$ is increased until panel failure ($\lambda_2 = \lambda_2^f$). The goal therefore is to maximize the in-plane compressive failure load by introducing λ_2^f as an objective function. Two aspect ratios are investigated: $a/b = 1$ and $a/b = 2$.

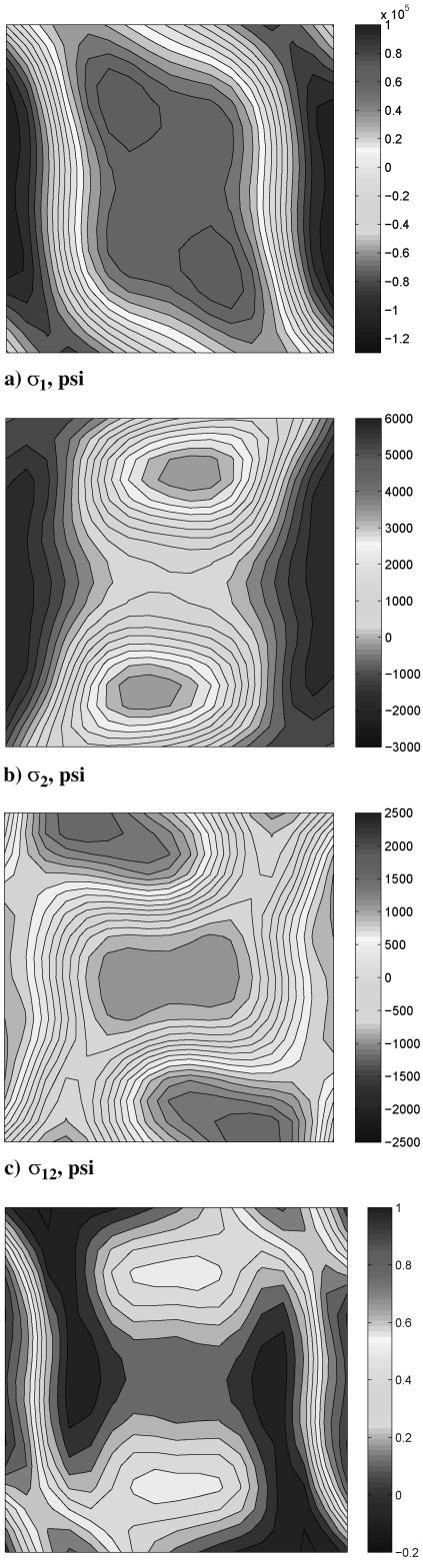

Fig. 11 Stresses and failure index in the upper layer for constant-stiffness design; $\lambda_1^f = 5.56$.

For the square panel, the best straight-fiber design is for a laminate with $[\pm 62\,\text{deg}]_{4s}$ stacking sequence, and the corresponding compressive failure load is $\lambda_2^f = 1.911$. For the variable-stiffness design, the fiber orientation is varied spatially as a function of x and y, $\theta = \theta(x, y)$, using different numbers of design variables. A comparison between the constant-stiffness and the variable-stiffness designs for different numbers of design variables is shown in Table 4. For the variable-stiffness designs, the optimal fiber-orientation

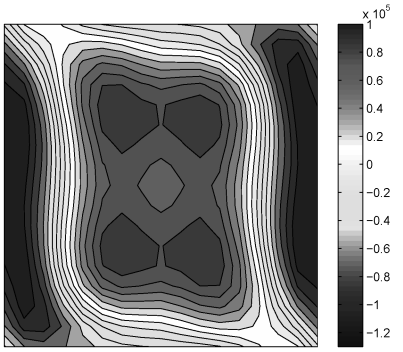

a) σ_1, psi

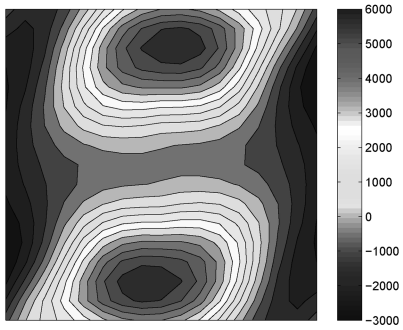

b) σ_2, psi

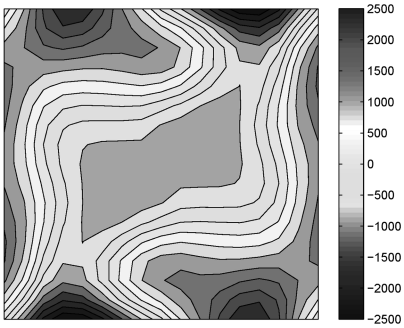

c) σ_{12}, psi

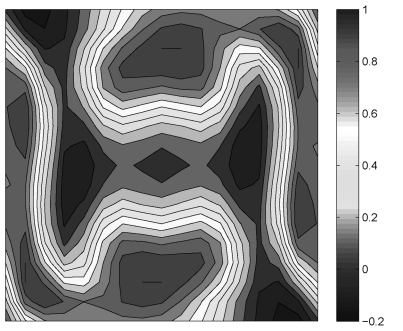

d) Failure index

Fig. 12 Stresses and failure index in the upper layer for variable-stiffness design; $\lambda_1^f = 7.43$.

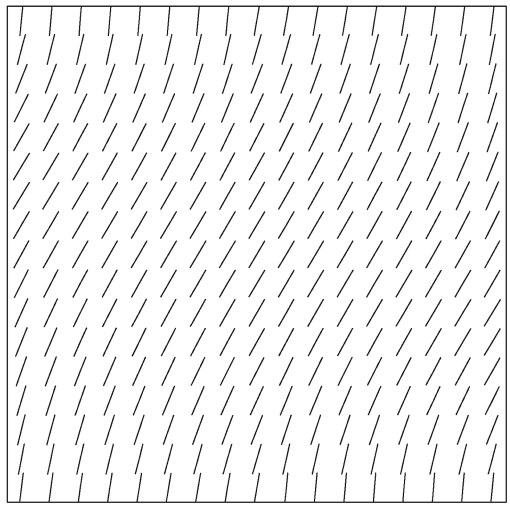

Fig. 13 Case-II optimal distribution of the fiber-orientation angles for maximum failure load; $m = 4$, $n = 7$, and $a/b = 1$.

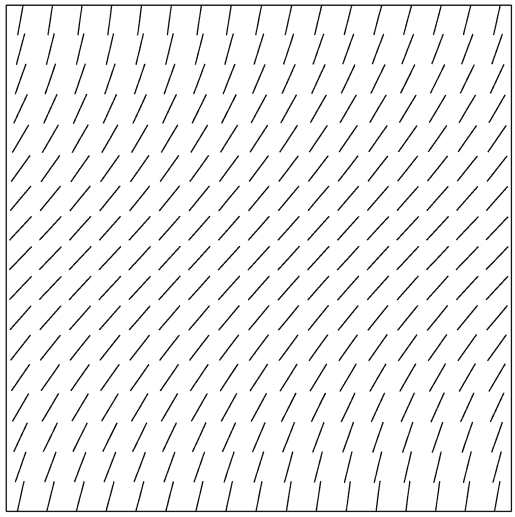

Fig. 14 Case-II optimal distribution of the fiber-orientation angles for maximum failure load; $m = 4$, $n = 9$, and $a/b = 1$.

distributions for the developed designs are depicted in Figs. 13 and 14. The optimal fiber paths obtained by using the streamline analogy for $m = 4$ and $n = 9$ are illustrated in Fig. 15. The maximum failure load obtained using 4×9 coefficients provides a load-carrying-capacity improvement of more than 15% over the optimal straight-fiber design. Note that the fiber paths are smooth, exhibiting neither discontinuities nor large curvatures. This makes the obtained designs efficient and feasible to be manufactured.

For the rectangular panel with $a/b = 2$, the results are summarized in Table 5 for the constant-stiffness and the variable-stiffness designs, and the optimal distribution of the fiber-orientation angles and the corresponding fiber paths for the variable-stiffness designs are shown in Figs. 16 and 17.

It is apparent that compared with the square panel, a larger improvement can be achieved in the load-carrying capacity. For the panel with an aspect ratio of 2, a maximum gain of 26.6% is obtained,

Table 4 Case-II load-carrying-capacity improvement (steered fiber vs straight fiber); $\theta = \theta(x, y)$ and $a/b = 1$.

Design type	No. of design variables, $m \times n$	Failure load λ_2^f	Load-carrying capacity improvement, %
Constant stiffness $[\pm 62\,\text{deg}]_{4s}$	——	1.911	——
Variable stiffness	4×7	2.072	7.9
Variable stiffness	4×9	2.257	15.3

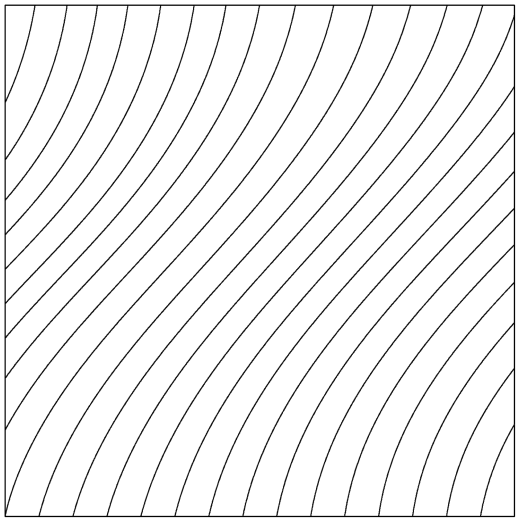

Fig. 15 Case-II optimal fiber paths for maximum failure load; $m = 4$, $n = 9$, and $a/b = 1$.

compared with the straight-fiber design. It can also be observed that by increasing the number of design variables, the fiber paths curve more, resulting in large curvatures that are unfavorable from the manufacturability point of view. These large curvatures can traditionally be avoided by imposing constraints on the radius of curvature of the fiber paths in the optimization process. However, it is obvious that by simply considering a smaller number of design variables, as is the case for $m = 4$ and $n = 7$, the fiber paths may be maintained smooth, as shown in Fig. 16.

VII. Conclusions

In this paper, design tailoring for the pressure-pillowing problem of a fuselage skin panel using tow-placed steered fibers was demonstrated. The problem was modeled as a two-dimensional plate using von Kármán plate equations, and the nonlinear analysis was performed using the Rayleigh–Ritz method. Optimal fiber paths defined parametrically over the structure were determined for maximum failure load. Optimal designs for both straight fibers and steered fibers were obtained for different loading cases and different aspect ratios. It was shown that by placing the fibers in their optimal spatial orientations, the pressure-pillowing problem can be alleviated and the load-carrying capacity of the structure can be improved, compared with traditional designs with straight fibers. The increase in the load-carrying capacity over the constant-stiffness design obtained for the variable-stiffness design was mainly due to the stress redistribution throughout the panel, achieved by the steered fibers. It was also shown that as the aspect ratio of the panel increases, more improvement in the load-carrying capacity can be achieved. Linear and nonlinear functions were used to describe the variation of the fiber-orientation angles. Nonlinear variations offered more flexibility for the laminate tailoring, thus showing better performance and proving the limitation of using linear variation of fiber orientations. Fiber paths corresponding to the optimal designs appeared to be smooth curves with small curvatures, suggesting the feasibility of fabrication of the designs using advanced tow-placement machines.

In this study, one ply was designed using the steered fibers (i.e., $[\pm\theta]_{ns}$). However, in general, each ply of the laminate can be designed to have its own fiber-orientation distribution, for instance, a

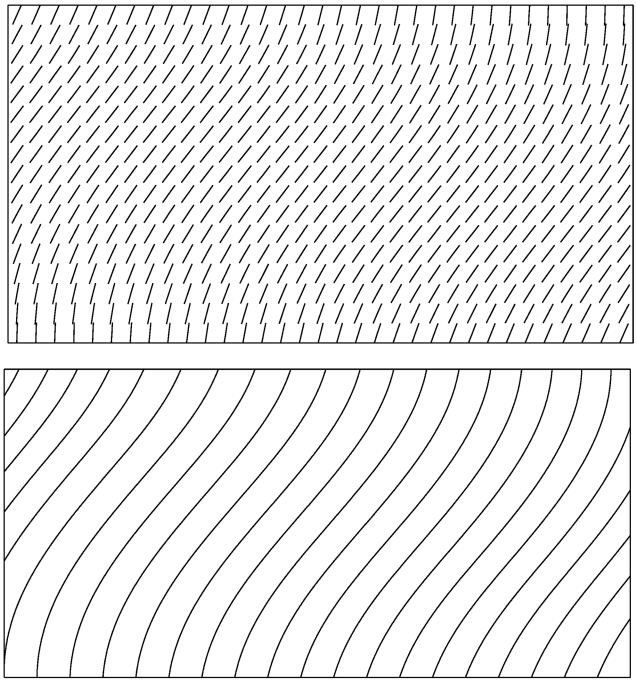

Fig. 16 Case-II optimal distribution of the fiber-orientation angles for maximum failure load and the corresponding fiber paths; $m = 4$, $n = 7$, and $a/b = 2$.

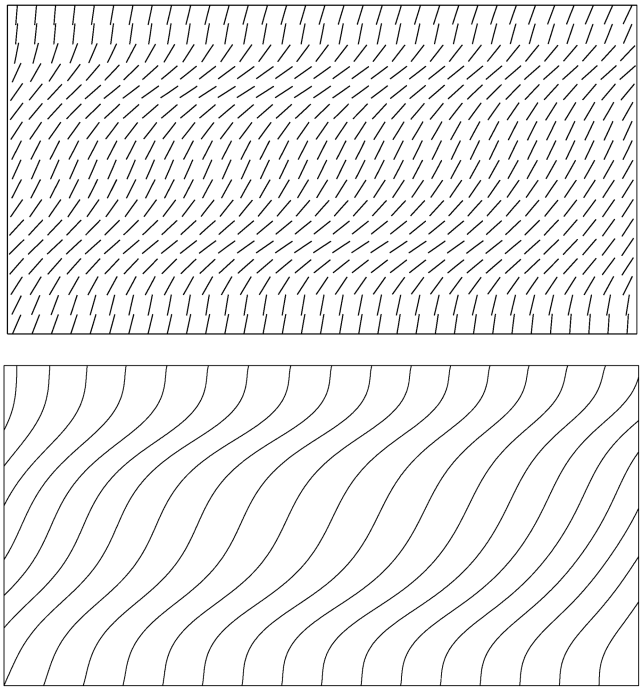

Fig. 17 Case-II optimal distribution of the fiber-orientation angles for maximum failure load and the corresponding fiber paths; $m = 4$, $n = 9$, and $a/b = 2$.

Table 5 Case-II load-carrying-capacity improvement (steered fiber vs straight fiber); $\theta = \theta(x, y)$and $a/b = 2$.

Design type	No. of design variables, $m \times n$	Failure load λ_2^f	Load-carrying capacity improvement, %
Constant stiffness $[\pm 60\ \text{deg}]_{4s}$	——	1.930	——
Variable stiffness	4×7	2.252	14.3
Variable stiffness	4×9	2.630	26.6

balanced variable-stiffness laminate with $[\pm\theta_1 \pm \theta_2 \cdots \pm \theta_n]_s$ layup. Unbalanced laminates can also be designed by including the terms A_{16} and A_{26} in Eq. (6). Although this may improve the laminate performance substantially, the dimension of the design space grows as the number of layers is increased, thus significantly increasing the computational cost of obtaining the optimal design.

Finally, the fuselage skin was modeled as a flat panel in this work. However, such a panel is normally modeled as a shallow shell. This will be addressed, along with panels with window openings, in the next step of this research.

Appendix: Laminated Plate Analysis

The in-plane and the bending stiffnesses are given as

$$A_{ij} = \sum_{k=1}^{N} \bar{Q}_{ij}^{(k)} (Z_{k+1} - Z_k) \qquad D_{ij} = \frac{1}{3} \sum_{k=1}^{N} \bar{Q}_{ij}^{(k)} (Z_{k+1}^3 - Z_k^3)$$

The transformed reduced stiffnesses of an orthotropic layer at angle θ is given as

$$\begin{aligned}
\bar{Q}_{11} &= U_1 + U_2 \cos 2\theta + U_3 \cos 4\theta \\
\bar{Q}_{12} &= U_4 - U_3 \cos 4\theta \\
\bar{Q}_{22} &= U_1 - U_2 \cos 2\theta + U_3 \cos 4\theta \\
\bar{Q}_{16} &= \tfrac{1}{2} U_2 \sin 2\theta + U_3 \sin 4\theta \\
\bar{Q}_{26} &= \tfrac{1}{2} U_2 \sin 2\theta - U_3 \sin 4\theta \\
\bar{Q}_{66} &= \tfrac{1}{2}(U_1 - U_4) - U_3 \cos 4\theta
\end{aligned}$$

The invariants are given as

$$\begin{aligned}
U_1 &= \tfrac{1}{8}(3Q_{11} + 3Q_{22} + 2Q_{12} + 4Q_{66}) \\
U_2 &= \tfrac{1}{2}(Q_{11} - Q_{22}) \\
U_3 &= \tfrac{1}{8}(Q_{11} + Q_{22} - 2Q_{12} - 4Q_{66}) \\
U_4 &= \tfrac{1}{8}(Q_{11} + Q_{22} + 6Q_{12} - 4Q_{66})
\end{aligned}$$

The reduced stiffnesses of the orthotropic layers are given in terms of the engineering constants of the material as

$$Q_{11} = \frac{E_1}{1 - \upsilon_{12}\upsilon 21} \qquad Q_{12} = \frac{\upsilon_{12} E_2}{1 - \upsilon_{12}\upsilon 21} = \frac{\upsilon_{21} E_1}{1 - \upsilon_{12}\upsilon 21}$$

$$Q_{22} = \frac{E_2}{1 - \upsilon_{12}\upsilon 21} \qquad Q_{66} = G_{12}$$

The terms used in Eqs. (10) are as follows:

$$K_{il}^{ub} = \int_0^a \int_0^b (A_{11} \Phi_{i,x}^u \Phi_{l,x}^u + A_{66} \Phi_{i,y}^u \Phi_{l,y}^u)\, \mathrm{d}x\, \mathrm{d}y$$

$$K_{il}^{uc} = \int_0^a \int_0^b (A_{12} \Phi_{i,y}^v \Phi_{l,x}^u + A_{66} \Phi_{i,x}^v \Phi_{l,y}^u)\, \mathrm{d}x\, \mathrm{d}y$$

$$\begin{aligned}
K_{ijl}^{uaa} = \frac{1}{2} \int_0^a \int_0^b (&A_{11} \Phi_{i,x}^w \Phi_{j,x}^w \Phi_{l,x}^u + A_{12} \Phi_{i,y}^w \Phi_{j,y}^w \Phi_{l,x}^u \\
&+ A_{66} \Phi_{i,x}^w \Phi_{j,y}^w \Phi_{l,y}^u + A_{66} \Phi_{i,y}^w \Phi_{j,x}^w \Phi_{l,y}^u)\, \mathrm{d}x\, \mathrm{d}y
\end{aligned}$$

$$K_{il}^{vb} = \int_0^a \int_0^b (A_{12} \Phi_{i,x}^u \Phi_{l,y}^v + A_{66} \Phi_{i,y}^u \Phi_{l,x}^v)\, \mathrm{d}x\, \mathrm{d}y$$

$$K_{il}^{vc} = \int_0^a \int_0^b (A_{22} \Phi_{i,y}^v \Phi_{l,y}^v + A_{66} \Phi_{i,x}^v \Phi_{l,x}^v)\, \mathrm{d}x\, \mathrm{d}y$$

$$\begin{aligned}
K_{ijl}^{vaa} = \frac{1}{2} \int_0^a \int_0^b (&A_{12} \Phi_{i,x}^w \Phi_{j,x}^w \Phi_{l,y}^v + A_{22} \Phi_{i,y}^w \Phi_{j,y}^w \Phi_{l,y}^v \\
&+ A_{66} \Phi_{i,x}^w \Phi_{j,y}^w \Phi_{l,x}^v + A_{66} \Phi_{i,y}^w \Phi_{j,x}^w \Phi_{l,x}^v)\, \mathrm{d}x\, \mathrm{d}y
\end{aligned}$$

$$\begin{aligned}
K_{il} = \int_0^a \int_0^b (&D_{11} \Phi_{i,xx}^w \Phi_{l,xx}^w + D_{12} \Phi_{i,yy}^w \Phi_{l,xx}^w + D_{12} \Phi_{i,xx}^w \Phi_{l,yy}^w \\
&+ D_{22} \Phi_{i,yy}^w \Phi_{l,yy}^w + 2D_{16} \Phi_{i,xx}^w \Phi_{l,xy}^w + 2D_{16} \Phi_{i,xy}^w \Phi_{l,xx}^w \\
&+ 2D_{26} \Phi_{i,yy}^w \Phi_{l,xy}^w + 2D_{26} \Phi_{i,xy}^w \Phi_{l,yy}^w + 4D_{66} \Phi_{i,xy}^w \Phi_{l,xy}^w)\, \mathrm{d}x\, \mathrm{d}y
\end{aligned}$$

$$\begin{aligned}
K_{ikl}^{wba} = \int_0^a \int_0^b (&A_{11} \Phi_{i,x}^u \Phi_{k,x}^w \Phi_{l,x}^w + A_{12} \Phi_{i,x}^u \Phi_{k,y}^w \Phi_{l,y}^w \\
&+ A_{66} \Phi_{i,y}^u \Phi_{k,y}^w \Phi_{l,x}^w + A_{66} \Phi_{i,y}^u \Phi_{k,x}^w \Phi_{l,y}^w)\, \mathrm{d}x\, \mathrm{d}y
\end{aligned}$$

$$\begin{aligned}
K_{ikl}^{wca} = \int_0^a \int_0^b (&A_{12} \Phi_{i,y}^v \Phi_{k,x}^w \Phi_{l,x}^w + A_{22} \Phi_{i,y}^v \Phi_{k,y}^w \Phi_{l,y}^w \\
&+ A_{66} \Phi_{i,x}^v \Phi_{k,y}^w \Phi_{l,x}^w + A_{66} \Phi_{i,x}^v \Phi_{k,x}^w \Phi_{l,y}^w)\, \mathrm{d}x\, \mathrm{d}y
\end{aligned}$$

$$\begin{aligned}
K_{ijkl}^{waaa} = \frac{1}{2} \int_0^a \int_0^b (\, &A_{11} \Phi_{i,x}^w \Phi_{j,x}^w \Phi_{k,x}^w \Phi_{l,x}^w + A_{12} \Phi_{i,y}^w \Phi_{j,y}^w \Phi_{k,x}^w \Phi_{l,x}^w \\
&+ A_{12} \Phi_{i,x}^w \Phi_{j,x}^w \Phi_{k,y}^w \Phi_{l,y}^w + A_{22} \Phi_{i,y}^w \Phi_{j,y}^w \Phi_{k,y}^w \Phi_{l,y}^w \\
&+ A_{66} \Phi_{i,x}^w \Phi_{j,y}^w \Phi_{k,y}^w \Phi_{l,x}^w + A_{66} \Phi_{i,x}^w \Phi_{j,y}^w \Phi_{k,x}^w \Phi_{l,y}^w \\
&+ A_{66} \Phi_{i,y}^w \Phi_{j,x}^w \Phi_{k,y}^w \Phi_{l,x}^w + A_{66} \Phi_{i,y}^w \Phi_{j,x}^w \Phi_{k,x}^w \Phi_{l,y}^w)\, \mathrm{d}x\, \mathrm{d}y
\end{aligned}$$

$$\mathrm{P}_l = \int_0^a \int_0^b p \Phi_l^w\, \mathrm{d}x\, \mathrm{d}y$$

References

[1] Biggers, S. B., and Srinivasan, S., "Compression Buckling Response of Tailored Rectangular Composite Plates," *AIAA Journal*, Vol. 31, No. 3, 1993, pp. 590–596.

[2] Biggers, S. B., and Pageau, S. S., "Shear Buckling Response of Tailored Rectangular Composite Plates," *AIAA Journal*, Vol. 32, No. 5, 1994, pp. 1100–1103.

[3] Gürdal, Z., and Olmedo, R. A., "Composite Laminates with Spatially Varying Fiber Orientations: Variable-Stiffness Panel Concept," *33rd Structures, Structural Dynamics and Materials Conference*, Vol. 2, AIAA, Reston, VA, 1992, pp. 798–808.

[4] Tatting, B. F., and Gürdal, Z., "Enhancements of Tow-Steering Design Techniques: Design of Rectangular Panel Under Combined Loads," NASA CR-2005-213911, Sept. 2005.

[5] Jegley, D., Tatting, B., and Gürdal, Z., "Tow- Steered Panels with Holes Subjected to Compression or Shear Loads," 46th AIAA/ASME/AHS/ASC Structures, Structural Dynamics, and Materials Conference, Austin, TX, AIAA Paper 2005-2081, 18–21 Apr. 2005.

[6] Tatting, B. F., and Gürdal, Z., "Automated Finite Element Analysis of Elastically-Tailored Plates," NASA CR-2003-212679, Dec. 2003.

[7] Setoodeh, S., Abdalla, M. M., and Gürdal, Z., "Design of Variable-Stiffness Laminates Using Lamination Parameters," *Composites, Part B*, Vol. 37, Nos. 4–5, 2006, pp. 301–309. doi:10.1016/j.compositesb.2005.12.001

[8] Setoodeh, S., Blom, A. W., Abdalla, M. M., and Gürdal, Z., "Generating Curvilinear Fiber Paths from Lamination Parameters Distribution," 47th AIAA/ASME/ASCE/AHS/ASC Structures, Structural Dynamics, and Materials Conference, Newport, RI, AIAA Paper 2006-1875, 2006.

[9] Boitnott, R. L., Starnes, J. H. Jr., and Johnson, E. R., "Nonlinear Response and Failure of Pressurized Composite Curved Panels," *Journal of Aerospace Engineering*, Vol. 8, No. 3, July 1995, pp. 129–138. doi:10.1061/(ASCE)0893-1321(1995)8:3(129)

[10] Alhajahmad, A., Abdalla, M. M., and Gürdal, Z., "Design Tailoring for Pressure Pillowing Using Tow-Placed Steered Fibers," *38th International SAMPE Technical Conference* [CD-ROM], Society for the Advancement of Material and Processing Engineering, Covina, CA, 6–9 Nov. 2006.

[11] Watson, L. T., Sosonkina, M., Melville, R. C., Morgan, A. P., and Walker, H. F., "Algorithm 777: HOMPACK90: A Suite of Fortran 90 Codes for Globally Convergent Homotopy Algorithm," *ACM Transactions on Mathematical Software*, Vol. 23, No. 4, Dec. 1997, pp. 514–549. doi:10.1145/279232.279235

[12] Reddy, J. N., *Mechanics of Laminated Composite Plates*, Theory and Analysis, CRC Press, Boca Raton, FL, 1997, Chap. 3.

[13] Chia C.-Y., *Nonlinear Analysis of Plates*, McGraw–Hill, New York, 1980, Chap. 3.

[14] Ragon, S. A., Gürdal, Z., and Watson, L. T., "Comparison of Three Algorithms for Tracing Nonlinear Equilibrium Paths of Structural Systems," *41st AIAA/ASME/ASCE/AHS/ASC Structures, Structural Dynamics, and Materials Conference*, Vol. 1, AIAA, Reston, VA, 2000, pp. 850–860.

[15] Jones R., M., *Mechanics of Composite Materials*, 2nd ed., Taylor and Francis, Philadelphia, 1998, Chap. 2.

[16] Blom, A. W., Abdalla, M. M., and Gürdal, Z., "Optimization of Tow-Placed, Tailored Composite Laminates," *16th International Conference on Composite Materials* [CD-ROM], Japan Society for Composite Materials, Tokyo, Japan, 8–13July 2007.